Journal of Materials Chemistry A

Dynamic Article Links ▶

PAPER

Acetoacetanilide functionalized Fe_3O_4 nanoparticles for selective and cyclic removal of Pb^{2+} ions from different charged wastewaters.

R. K. Sharma,*[a] Aditi Puri[a], Yukti Monga[a], and Alok Adholeya[b]

Efficienct, selective and reusable acetoacetanilide functionalized Fe_3O_4 nanoparticles for the removal of Pb^{2+} ions, were developed for the first time. A comprehensive characterization of the functionalized nanoparticles, at different levels of synthesis, was carried out by TEM, EDS, XRD, SEM, FT-IR and VSM. The adsorption equilibrium obeyed Langmuir isotherm model with the maximum enrichment
10 capacity of 392.2 mgg^{-1} at 318 K. Pb^{2+} ions showed quick removal, and adsorption rate followed pseudo second-order kinetics. In addition, isotherm and kinetic studies suggested that adsorption process is controlled by chemical adsorption involving complexation of metal ions with the functional groups present on the surface of functionalized nanoparticles. The thermodynamic analysis revealed that the analyte adsorption is spontaneous, endothermic and energetically driven in nature. Due to
15 superparamagnetism of the Fe_3O_4 nanoparticles as magnetic core and silica coat serving as a protection shell, the adsorbent was easily separated and effectively recycled without significant deterioration in its original performance for at least 10 continuous usage. Furthermore, the proposed environmentally benign analytical process was successfully applied for the selective recovery of Pb^{2+} ions from different charged wastewater.

20 ## Introduction

There is no doubt that industrialization has given a fascinating outlook to the society. However, its accelerated pace without commensurate safeguard mechanisms has led to the insidious consequences. The failure of this unregulated growth can be
25 observed by the current alarming rates of metal inputs, which has pushed the humanity towards environmental and health complexities.[1] Besides this, it has caused excessive depletion of resources and raised a key concern regarding their availability in the near future. It is predicted that if the current rate of exhaustion
30 continues, we will soon become resource deficit.[2,3] For e.g. having a wide usage with modern technology and industries, lead is one of the most valuable commodities in the present scenario.[4,5] The seemingly valuable properties of this metal have given profitable directions to the popular professional sectors, but
35 simultaneously, the current practice rate and urban runoffs have resulted in large reserve depletion and environmental disposal in an inaccessible manner. Moreover, its excessive deposition in various ecological compartments is pushing the modern society towards health related complications, as the metal finds no basic
40 role in the orderly continuation of life.[6,7]

So far, adsorption, membrane separation technology, ion exchange, chemical treatment and electrochemical methods have been employed for the removal of Pb^{2+} ions.[1] Among them, adsorption is one of the best available technologies due to its
45 convenient operation process, wide applicability, high efficiency,

low energy requirement and cost effectiveness.[7,8] In this perspective, nano sized materials have nowadays gained much attention because of their unique properties like high surface areas, enhanced active sites and excellent sorption capacities.[9]
50 Bayazit and Inci investigated the adsorption of Pb^{2+} on carbon nanotubes oxidized by different methods.[10] In other studies, the adsorptive performance of polymer-based graphene oxide nanocomposites[1] and graphene oxide nanosheets[11] towards Pb^{2+} ions were explored. Though, the sorption efficiency of the
55 adsorbents were remarkably high, their profitable utilization is hindered due to the drawbacks like cumbersome synthesis and separation strategy, secondary wastes generation, and lack of stability and reusability.

On the other hand, silica coated iron oxide based
60 nanomaterials have paved the way for their widespread acceptance owing to their ease of separation, environmentally benign and inexpensive nature of the embedded core, repetitive use, outstanding chemical and mechanical stability endowed by impenetrable protective layer and large specific surface area.[12-14]
65 Furthermore, these magnetically responsive nanoparticles allow simple and facile recovery and recycling of the metals, which is deemed an essential feature to close the resource/waste loop.[15] So, fabrication of these nanomaterials is currently undergoing exciting developments with increasing achievements for Pb^{2+}
70 adsorption. The research group of Zhang reported silica based core–shell nanomaterial prepared *via* a controllable sol–gel

Journal of Materials Chemistry A Accepted Manuscript

process as an efficient adsorbent for Pb^{2+} removal.[16] Similarly, Ren and co-workers synthesized magnetic EDTA-modified chitosan/SiO$_2$/Fe$_3$O$_4$ nanoparticles with enhanced reusable characteristics.[17] However, these functionalized nanoadsorbents

5 are nonspecific and exhibit low selectivity, which is one of the major challenges in the field of adsorption and is generally limited to ion imprinted polymers. For e.g., Cui *et al.* prepared well-defined surface ion-imprinted magnetic microspheres, which displayed selective binding capability for the Pb^{2+} ions.[18]

10 Likewise, magnetic ion-imprinted polymer (Fe$_3$O$_4$@SiO$_2$-IIP) synthesized by Guo and group showed exclusive selectivity for Pb^{2+}.[19] But, from a practical point of view, very low uptake capacities limit their application. Very recently, Chen's group reported double silica layer structured magnetic microspheres for

15 selective recognition of Pb^{2+} using host guest chemistry, but the material suffer from low adsorption capacity and high equilibration time for metal removal. Besides, it could not be reutilized for more than three successive adsorption-desorption cycles.[20] Hence, there is an urgency to develop highly stable

20 functionalized magnetic nanoparticles, which can offer opportunities to reduce energy usage, minimize waste disposal and conserve resources *via* convenient, efficient, selective and repetitive recovery of Pb^{2+} ions.

Experimental section

25 **Motivation and strategy**

Considering the scarcity of the sustainable methods integrating efficiency, selectivity and reusability on a single platform, herein, we report, novel acetoacetanilide functionalized Fe$_3$O$_4$ nanoparticles for the removal of Pb^{2+} ions from different charged

30 wastewaters including mycorrhizal treated fly-ash. Though, various ligands have been used for surface modifications of nanoparticles to improve their sorption capacity and selectivity,[17,21] but no studies have, to date, explored the possibility of using acetoacetanilide (AAA) as organosubstituent

35 for metal removal. In fact, based on the environmental fate and eco-toxicological properties, AAA is nontoxic to the aquatic environment, and can be incorporated easily for the desired purpose. Besides this, concerning the atmospheric deterioration caused due to the seepage of toxic Pb^{2+} ions from fly-ash into

40 local surroundings, the novel and unique applicability of the presented protocol can assist in continuous monitoring and timely removal of Pb^{2+} ions from fly-ash, which is much required to cease its surplus transfer into the biota.

Synthesis of acetoacetanilide functionalized Fe$_3$O$_4$
45 **nanoparticles (AAA-NH$_2$-Si@MNPs)**

The synthesis of Fe$_3$O$_4$ magnetic nanoparticles (MNPs), their subsequent silica shell coating, (Si@MNPs) and further immobilization with APTES (NH$_2$-Si@MNPs) was performed as described in our previous work.[13] For the covalent

50 functionalization of AAA with NH$_2$-Si@MNPs, their mixture was refluxed in ethanol solution for 2 h. The resultant acetoacetanilide functionalized Fe$_3$O$_4$ nanoparticles (AAA-NH$_2$-Si@MNPs) were separated magnetically, washed with ethanol, water and dried under vacuum.
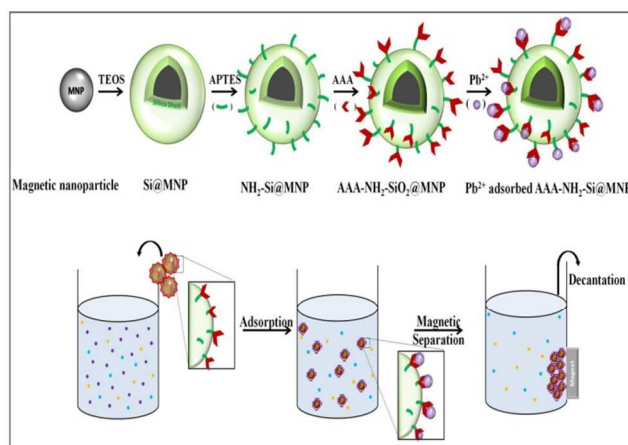
Scheme 1 Schematic illustration of the synthetic route of AAA-NH$_2$-Si@MNPs followed by Pb^{2+} removal sequence.

Batch adsorption experiments

To investigate the adsorption behaviour at different pH, 0.05 g
60 portions of AAA-NH$_2$-Si@MNPs were suspended in 50.0 mL of sample solutions, containing 25 mgL^{-1} Pb^{2+} at room temperature, pre-adjusted to the pH values 2-6 using 0.01-0.1 M NaOH/HCl. To facilitate the adsorption of metal on the functionalized surface of nanoparticles, the suspension was sonicated for 2 min before

65 being subjected to the shaking process. After reaching the adsorption equilibrium, a permanent magnet was set beside to move the metal adsorbed AAA-NH$_2$-Si@MNPs to the wall (Figure ESI-S1), allowing easy decantation of the supernatant liquid (Scheme 1). The residual concentration of the metal ions in

70 the supernatant was analysed using FAAS. The amount of Pb^{2+} adsorbed per unit mass of adsorbents (mgg^{-1}) was evaluated according to the following equation

$$Q = \frac{(C_o - C_e)V}{w} \qquad (1)$$

where, C_0 and C_e (mgL^{-1}) are initial and final Pb^{2+} concentrations
75 in solution, V (L) is the volume of the Pb^{2+} solution, and w (g) is the weight of dried AAA-NH$_2$-Si@MNPs.

Adsorption capacity and isotherm experiments were carried out with 50 mL analyte solutions ranging from 50 to 400 mgL^{-1} at different temperatures: 298, 308 and 318 K. For the adsorption

80 kinetic equilibrium study, treatment time was varied from 5 min to 30 min. The suspension sample was taken out at different contact times, and after the separation of metal loaded adsorbent, the residual Pb^{2+} concentration in the clear solution was analyzed.

Results and discussion

85 **Characterizations of AAA-NH$_2$-Si@MNPs**

Shape, morphology and purity of nanoparticles

The shape, size and morphological characteristics of MNPs before and after surface modifications were investigated by Transmission electron microscopy (TEM) and Scanning electron

90 microscopy (SEM). The TEM image of synthesized nanocore apparently defines the uniform structure of the MNPs with an average size in between 8-12 nm. Their crystalline nature is confirmed by the presence of an array of the bright diffraction rings, which come from the planes of magnetite in the selected-

95 area electron diffraction (SAED) pattern (Figure 1). In addition,

the high resolution TEM (HRTEM) image shows clear 2D lattice fringes of the magnetite material. The interplanar spacing is about 0.3 nm, which corresponds well to the (2 2 0) lattice plane of the inverse spinel structure of Fe_3O_4. After coating process, the presence of silica layer of around 3-5 nm can be easily seen at the periphery of MNPs. This core-shell feature elucidates that the Fe_3O_4 nanoparticles are well embedded inside rather than simply adhering physically or blending into the silica. The deposition of organic polymer (APTES) to the surface of Si@MNPs, is revealed by Figure 1d.
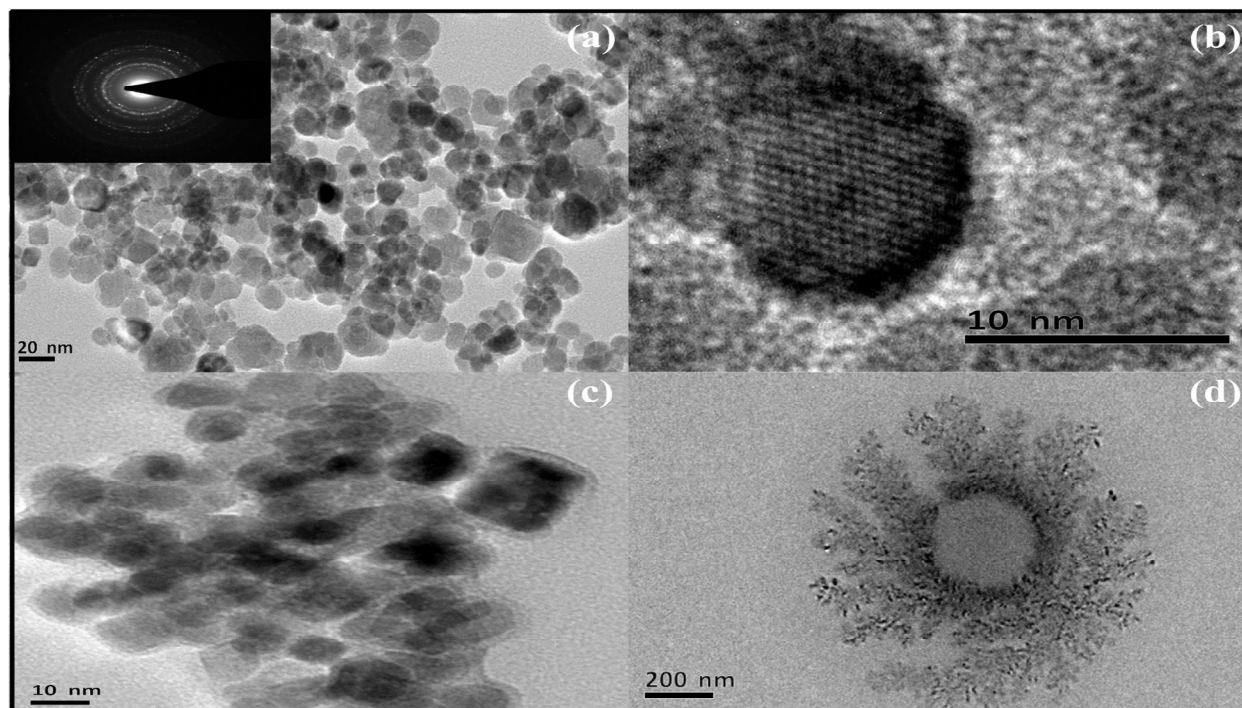
Fig.1 TEM images of the nanoparticles obtained at different stages of synthesis (a) MNPs, (b) HR-TEM image of MNPs, (c) Si@MNPs and (d) NH_2-Si@MNPs. Inset of (a) shows SAED pattern of MNPs.

The SEM image captured at high magnification shows the smooth surface of the magnetic nanocore (Figure ESI-S2). While after encapsulation, it turns out to be rough, due to the deposition of silica coat to MNPs, which form a uniform and continuous shell around them. In fact, the appearance of the AAA-NH_2-Si@MNPs was found to be similar as that of Si@MNPs. It implies that the silica surface efficiently retained stability and prohibited the agglomeration of the particles at the selected synthesis conditions.

Phase and structural determination

The surface state and phase composition of the functionalized nanoparticles were investigated by X-ray powder diffraction (XRD) (Figure ESI-S3). The six characteristic brag peaks obtained at 2θ region of 10–80° indicate a highly crystalline cubic inverse spinel structure of the Fe_3O_4 with high phase purity. These were marked by their corresponding indices at (2 2 0), (3 1 1), (4 0 0), (4 2 2), (5 1 1) and (4 4 0), for the crystallographic faces of magnetite (JCPDS card no. 19-6290).[22] The average size of MNPs was estimated approximately as 12.9 nm, from full width at half-maximum (fwhm) of the (3 1 1) plane using Debye-Scherrer relationship (Dhkl ¼ kl/ βcosθ) *via* line broadening in the pattern.

The diffractrogram pattern of Si@MNPs differs significantly with the bare magnetic nanoparticles. A single, broad and strong diffraction hump between 2θ = 15-24° confirms the presence of poorly crystalline silica shell. Further, due to this amorphous coat, the diffraction pattern of the pure magnetite structure becomes weaker compared with that of non shelled MNPs. As expected, after organic functionalization, there is a further decrease in the intensity with the corresponding broadening of the silica peak. It can be accredited to the lowering of scattering contrast between the walls of the silica framework and organic moiety attached over Si@MNPs and their respective synergistic effect. Besides, no noticeable reflection peak has been witnessed after deposition of complexing active sites. This implies that organic moieties are symmetrically distributed on the surface of functionalized nanoparticles, which can be the reason for their high adsorption efficiency. In addition, the existence of distinguishable and persistent pattern of magnetite structure, in the latter two cases, shows the crystalline phase stability.[23] This further signifies that the variable reaction conditions encountered during the subsequent surface modification reactions did not affect the topological structure and inherent properties of AAA-NH_2-Si@MNPs.

The EDS spectra of the isolated particles of Si@MNPs and NH_2-Si@MNPs are shown in Figure 2. Figure 2a illustrates that the product is comprised of Iron (Fe) and Oxygen (O), which is due to the existence of iron oxide nanoparticles. Besides, the presence of Silica (Si) along with the other two key elements clearly reflects that rather than forming individual particles, silica is well adhered over the magnetite surface, which corroborates the findings obtained from TEM analysis. Moreover, in Figure 2b, the appearance of a peak corresponding to N atom, along with simultaneous decrease and increase in Fe and Si content, provide

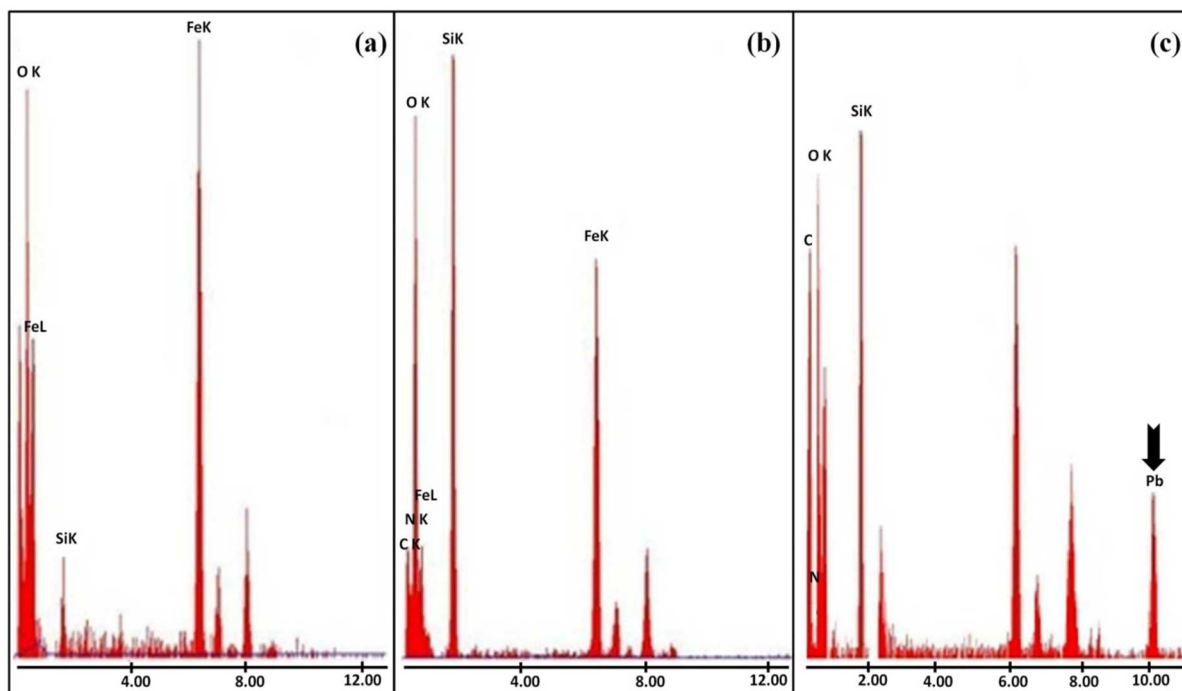the direct evidence of incorporation of APTES over Si@MNPs.

Fig.2 EDS spectra of (a) MNPs, (b) Si@MNPs and (c) Pb^{2+} adsorbed AAA-NH$_2$-Si@MNPs.

In the FTIR spectra, an intense band around 580 cm^{-1} is assigned to the typical Fe-O vibrations of the magnetite structure (Figure 3). The pronounced changes upon silica encapsulation can be identified by the appearance of Si-O-Si symmetric, Si-O symmetric and Si-O-Si asymmetric stretching modes observed at 798, 953 and 1090 cm^{-1} respectively, which are the characteristic absorption bands of amorphous silenous matrix.[24] In fact, Fe-O adsorption vibration in the same vicinity is decreased to lower intensity, which further verifies the surface coating of MNPs. Compared to Si@MNPs, in NH$_2$-Si@MNPs, the distinguishable peak of Si-OH stretch has been turned into a very weak shoulder signifying that the surface silanol groups are being substituted by aminosilane groups. Though, N-H vibration bands are not visible due to superposition to those with that of water at 1625 and in the 3300-3500 cm^{-1} range, but nevertheless, C-H stretch due to aminopropyl moiety is well noticed as an edge at 2926 cm^{-1}. The immobilization of ligand (AAA-NH$_2$-Si@MNPs) can be seen from the peak around 1609 cm^{-1} due to the C=N stretching vibration mode, suggesting the formation of covalent linkage *via* amine functionality.[15] Upon metal complexation, a noticeable shift of C=N and C=O frequencies to a lower wave number in conjunction with their decreased intensities elucidates the active role of these sites in the chemical adsorption of Pb^{2+} ions.

Property characterization

Figure 4 shows the saturation magnetization responses of the MNPs, Si@MNPs, AAA-NH$_2$-Si@MNPs powders upon application of various external magnetic fluxes from −20,000 to 20,000 Oe at room temperature. The superparamagnetic behaviour can be easily predicted from the inset, as the obtained plots show negligible coercivity and remanence in the absence of external magnetic field with both magnetization and demagnetization curves passing through the origin. Furthermore,

the saturation magnetization (Ms) of magnetite nanoparticles (53 emug^{-1}) is smaller than that of bulk magnetite (92 emug^{-1}).[25]
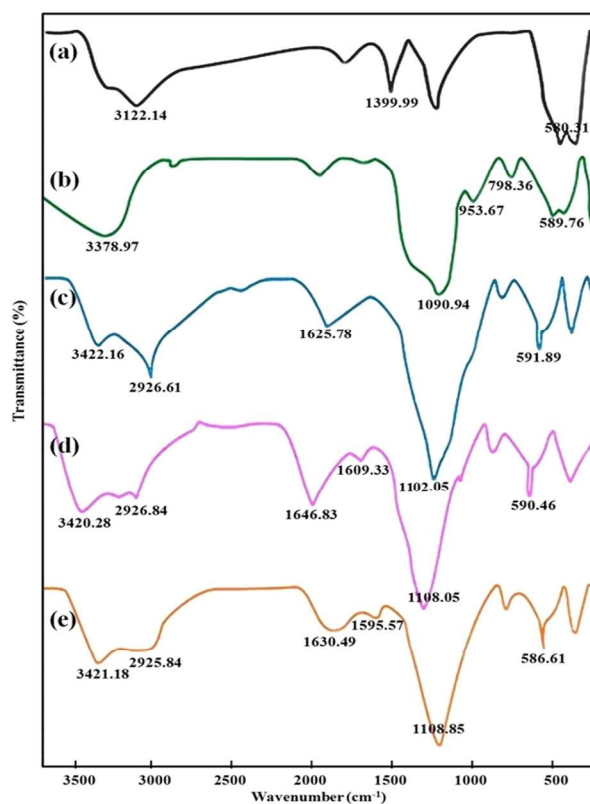

Fig.3 FT-IR spectra of (a) MNPs, (b) Si@MNPs, (c) NH$_2$-Si@MNPs, (d) AAA-NH$_2$-Si@MNPs and (e) Pb^{2+} adsorbed AAA-NH$_2$-Si@MNPs.

This decrease elucidates the precise role of particle size, which

is proportional to the extent of magnetization of a particle in an external applied field. Hence, smaller saturation magnetization value for the magnetic particles of nano range compared to bulk material is reasonable.
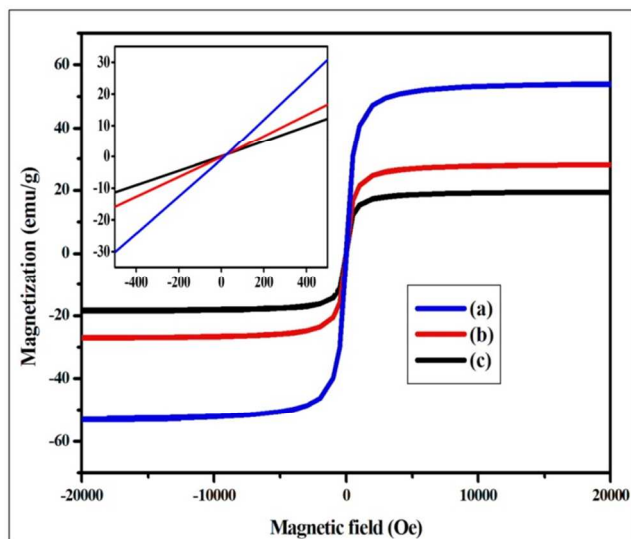
⁵ **Fig.4** Magnetic hysteresis loops of (a) MNPs, (b) Si@MNPs, (c) AAA-NH₂-Si@MNPs at room temperature. Inset shows enlargement of graph near origin.

After stabilization of the MNPs with silica (Si@MNPs)
¹⁰ followed by the covalent immobilization of the functional moieties (AAA-NH₂-Si@MNPs), Ms values are reduced to 28 $emug^{-1}$ and 19 $emug^{-1}$ respectively. This is undoubtedly related to the increase in surface disorder of MNPs *via* contribution of the non-magnetic silica shell, and the incorporated complexing
¹⁵ groups to the total mass of the nanoparticles.[26]

Effect of pH on lead adsorption and mechanism discussion

pH of the aqueous phase is an important parameter to be considered, as it can strongly affect the surface charge of the adsorbent. Besides, Pb^{2+} ions exist as different proportions of
²⁰ Pb^{2+}, $Pb(OH)^+$, $Pb(OH)_2^0$ and $Pb(OH)^{3-}$ at different pH values. In this study, the adsorption behaviour was investigated in the pH range of 2 to 6 as metal species predominantly remain as divalent free ions in the solution at pH < 6.[9,27] The curve representing the percentage adsorption as a function of initial pH is illustrated
²⁵ through Figure 5.

As can be seen, the AAA-NH₂-Si@MNPs show diminished affinity for metal adsorption at low pH values. This could be attributed to the three factors. First, in an acidic pH range, the surface functional groups are protonated to varied degrees. By
³⁰ this, the availability of active binding sites for the metal uptake is reduced to a greater extent. Second, due to the coloumbic repulsion between the positively charged surface and metal species bearing the same charge, the approach of metal ions to the nanoadsorbent is significantly hindered. Third, a high
³⁵ concentration of protons leads to a keen competition between analytes and hydrogen ions for the same binding sites.[17,28] Nevertheless, with the rise in pH value, the adsorption of Pb^{2+} ions increases sharply and reaches a plateau at pH 5. Similar trend is observed in zeta potential measurements at different pH
⁴⁰ values (Figure ESI-S4). It showed that the surface of

functionalized nanoparticles becomes negatively charged beyond the point of zero charge (P_{ZC}), which is around 3.9. This not only increases the density of active functional groups by deprotonation, but also enhances their availability to the metal
⁴⁵ cations by preventing the aggregation. Hence, all the succeeding investigations were performed at initial pH 5.
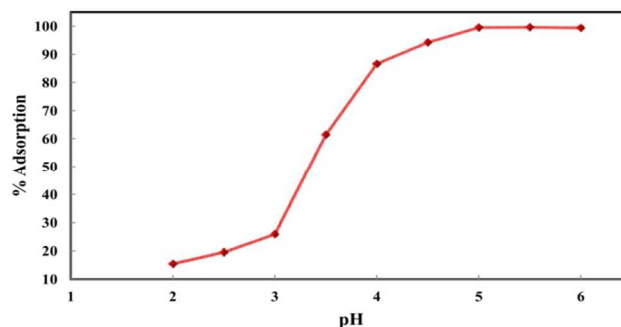
Fig.5 Effect of pH on the adsorption behaviour of AAA-NH₂-Si@MNPs for Pb^{2+} ions (Conditions: initial Pb^{2+} concentration: 50 mgL^{-1}, pH: 5.0,
⁵⁰ adsorbent dose: 1 gL^{-1}, contact time: 30 min, reaction temperature: 298 K).

The presence of metal in the adsorbent framework is witnessed by the existence of distinguishable and well resolved peak of Pb in the EDS spectrum (Figure 2c), which gave a pivotal
⁵⁵ evidence of metal adsorption at the desired pH.

To determine the coordination sites that may involve in complexation, FTIR spectra of the functionalized nanoparticles before and after metal adsorption (Figure 3d and 3e) were compared. As can be seen, the AAA-NH₂-Si@MNPs showed
⁶⁰ noticeable changes after binding to the Pb^{2+} ions. It exhibited the band of C=N in the region 1593-1597 cm^{-1} showing a bathochromic shift, which ensures the participation of nitrogen of the azomethine group in metal ion coordination. Moreover, the C=O band at 1646 cm^{-1} for the amide carbonyl group was shifted
⁶⁵ by 10-13 cm^{-1} to lower wavenumber, which signifies that the amide carbonyl oxygen is bonded to the Pb^{2+} ions. In fact, the intensities of the peaks are also weakened, which prove the active involvement of these sites for metal adsorption. Similar results have been observed in the previous reports of nanoadsorbents
⁷⁰ carrying these functional groups.[29-31] Hence, it is reasonable that amide carbonyl and imine functional groups posses the strong chelating ability for Pb^{2+} ions. It further implies that the covalent immobilization of acetoacetanilide over the surface of NH₂-Si@MNPs is strongly contributing to the efficient capturing of
⁷⁵ Pb^{2+} in the aqueous solution.

Adsorption kinetics

Effect of adsorption kinetics is an essential parameter to be studied as the removal rate directly affects the operation cost. It was found that the heavy metal ions uptake was very fast, and the
⁸⁰ process almost completely reached to the equilibrium within 30 min, which is much shorter than what has been reported previously.[14,16] The high adsorption rate can be attributed to the presence of sufficient adsorption sites, and ease of their accessibility as well as strong complexation ability towards Pb^{2+}
⁸⁵ ions. To check the suitable kinetic model with corresponding model parameters, the obtained data was formulated to the linearized form of pseudo first and second order models.

$$\ln(q_e - q_t) = lnq_e - k_1 t \tag{2}$$

$$\frac{t}{q_t} = \frac{1}{k_2 q_e^2} + \frac{t}{q_e} \tag{3}$$
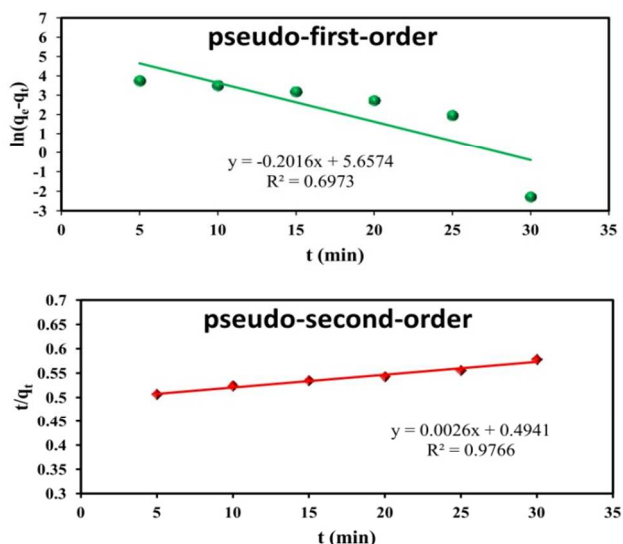
Fig.6 Linearized pseudo kinetic plots (a) first order and (b) second order for the adsorption of Pb^{2+} on AAA-NH$_2$-Si@MNPs.

The values of the obtained kinetic parameters are summarized in Table 1 and plots are depicted through Figure 6. As can be seen, the experimental value (q$_{exp}$) for pseudo-second order kinetic model is in good agreement with the calculated value (q$_e$). Besides, the high R^2 value shows the applicability of this model to describe the kinetic profile of the present system. Hence, it can be speculated that the adsorption rate is dependent only on the sorption capacity, but not the adsorbate concentration, while the sorption efficiency is directly linked to the number of active sites occupied on the adsorbent. It further indicates that the adsorption of Pb^{2+} ions onto AAA-NH$_2$-Si@MNPs is based on the chemisorption controlled rate of the process, involving the valence forces through sharing or exchange of electrons between metal ion and adsorbent.[32] Consequently, it is implied that the nature of interaction between adsorbent and Pb^{2+} ions is chemical, involving metal complexation as a dominant

mechanism, which correlates well with the results obtained from FTIR studies.[16]

Adsorption isotherms

Understanding the interaction behaviour between analyte and the adsorbent is of fundamental importance, and can be envisaged by employing different adsorption isotherms at pre-optimized conditions. In the present study, Langmuir and Freundlich adsorption isotherm models were used. Freundlich model assumes multilayer, reversible and non ideal adsorption at the active sites with exponential distribution of energies, which endorses the heterogeneity of the surface. Unlike Freundlich isotherm, Langmuir isotherm is based on monolayer and homogenized coverage of adsorbent surface, where all sorption sites are identical and energetically equivalent. The experimental equilibrium data at different temperatures were evaluated according to the linear equations of these models given underneath,[15] and the curve fitting results are complied in Table 2 (Figure ESI-S5 and S6).

$$\frac{C_e}{q_e} = \frac{1}{q_m K_L} + \frac{C_e}{q_m} \tag{4}$$

$$lnq_e = \frac{lnC_e}{n} + lnK_F \tag{5}$$

where, C$_e$ and q$_e$ are the concentration and adsorption capacity at equilibrium, and q$_m$ and K$_L$ are Langmuir constants represent the maximum adsorption capacity and energy of adsorption (Lmg^{-1}) respectively. K$_F$ and n are Freundlich constants related to adsorption capacity and intensity, respectively. Comparing the correlation coefficient, the Langmuir model yields a more accurate fit to the experimental data than Freundlich model. Further, it shows the clear consistency between calculated (q$_m$) and experimental values (q$_{exp}$) of the adsorption capacity at equilibrium. Therefore, it can be considered that the monolayer adsorption takes place at the specific sites present on the surface of AAA-NH$_2$-Si@MNPs, which are energetically identical. It further confirms that chemisorption occurs due to the complexation between Pb^{2+} ions and the organic groups present on the surface of nanoadsorbent.[6,7]

Table 1 Kinetic parameters and correlation coefficients for adsorption of Pb^{2+} on AAA-NH$_2$-Si@MNPs. (Conditions: initial Pb^{2+} concentration: 50 mgL^{-1}, pH: 5.0, adsorbent dose: 1 gL^{-1}, reaction temperature: 298 K)

Pseudo-first-order model $\ln(q_e - q_t) = lnq_e - k_1 t$			Pseudo-second-order model $\frac{t}{q_t} = \frac{1}{k_2 q_e^2} + \frac{t}{q_e}$		
q$_e$(q$_{exp}$)^a (mgg^{-1})	k$_1$ (min^{-1})	R^2	q$_e$(q$_{exp}$)^a (mgg^{-1})	k$_2$ ($\times 10^{-5}$ gmg^{-1}min^{-1})	R^2
286.4(380.1)	0.2016	0.6973	380.2(380.1)	1.39	0.9766

^{a} Experimental adsorption capacity value.

Adsorption thermodynamics

The improved sorption performance of the AAA-NH$_2$-Si@MNPs with elevated temperature elucidates that the adsorption process is thermodynamically driven. Thermodynamic parameters quantified with the measured data under a preset range of temperatures, are listed in Table 3. Figure ESI-S7 shows the plot of ln K$_L$ versus 1/T fitted to a straight line. The positive enthalpy

change found for the system reflects the endothermic nature of the process. This phenomenon is usually observed in the adsorption systems based on site specific interaction caused by the formation of chemical bonds between the surface of adsorbent and the heavy metal ions. Hence, adsorption process can be considered as chemisorption, because had it been only physisorption, the enthalpy of the system should have been exothermic. The positive ΔS value indicates the increase in

disorderness of the system, which comes from the release of water molecules surrounding the hydrated metal ions and solid-solution interface to the bulk aqueous medium during metal complexation process. Thereby, it results in preferential affinity of Pb^{2+} ions towards the adsorbent surface. The negative sign of ΔG implies spontaneity of the reaction, which comes from the difference between energetic potentials of the system components. It indicates that the binding energy of the metal-adsorbent is stronger than the metal-aqueous phase, which is considered as the driving force of the Pb^{2+} ions redistribution in the system and their rapid sorption onto the AAA-NH$_2$-Si@MNPs. The increase in negative magnitude of this parameter with the rise in experimental temperature demonstrates that the adsorption is more favourable at higher temperature, which eventually leads to the increase in adsorption efficiency. The acquired results are in agreement with previous studies on the adsorption of Pb^{2+} ions.[16,17]

Table 2 Langmuir and Freundlich isotherm constants, equilibrium parameters and correlation coefficients for adsorption of Pb^{2+} on AAA-NH$_2$-Si@MNPs (Conditions: initial Pb^{2+} concentration: 50 to 400 mgL^{-1}, pH: 5.0, adsorbent dose: 1 gL^{-1}, contact time: 30 min, reaction temperature: 298 K, 308K and 318K).

Isotherm Model	Estimated isotherm parameters	Temperature		
		298 K	308 K	318 K
Langmuir	R^2	0.9905	0.9735	0.9709
$\frac{C_e}{q_e} = \frac{1}{q_m K_L} + \frac{C_e}{q_m}$	q_m $(q_{exp})^a$	380.2(380.1)	389.1(386.1)	392.2 (392.4)
	K_L	0.822	0.988	1.214
	R_L	0.003-0.024	0.003-0.02	0.016-0.045
Freundlich	R^2	0.8595	0.9528	0.8122
$ln q_e = \frac{ln C_e}{n} + ln K_F$	K_F	147.6	188.3	184.9
	n	2.88	4.41	3.36

^{a} Experimental adsorption capacity value.

Table 3 Estimated values of thermodynamic parameters at different temperatures

| Temperature	ΔG (kJmol^{-1})	ΔH (kJmol^{-1})	ΔS (Jmol^{-1}K^{-1})
298 K	-29.84	15.36	151.65
308 K	-31.32		
318 K	-32.88		

Effect of the adsorbent dosage

The optimum amount of adsorbent greatly influences the process cost by minimizing the wastage and maximizing the quantitative recovery of heavy metal ions. Therefore, the optimal adsorbent dosage in terms of adsorption capacity of the functionalized nanoparticles was investigated at pH 6.0, by varying the adsorbent amount from 0.01 to 0.1 g.

Figure 7 illustrates that the 0.05 g of the AAA-NH$_2$-Si@MNPs is very much effective for the adsorption of Pb^{2+} ions. Beyond this, the adsorption capacity decreases remarkably. The observed trend can be explained on the basis of availability of binding sites, which rises with the increase in adsorbent dosage. However, the concentration of Pb^{2+} in the aqueous solution is fixed, and once nearly all the ions are adsorbed by the adsorbent, the number of vacant actives sites grows, which would no longer participate in the adsorption process.[17] This ultimately leads to a decrease in the adsorption capacity.

Desorption *via* ultrasonication and stability

To broaden the economic dimensions and practical significance of a nanoadsorbent for environmental purpose, its regeneration is highly desirable. Moreover, it aids in the effective separation and recovery of heavy metals for their reutilization or safe disposal.
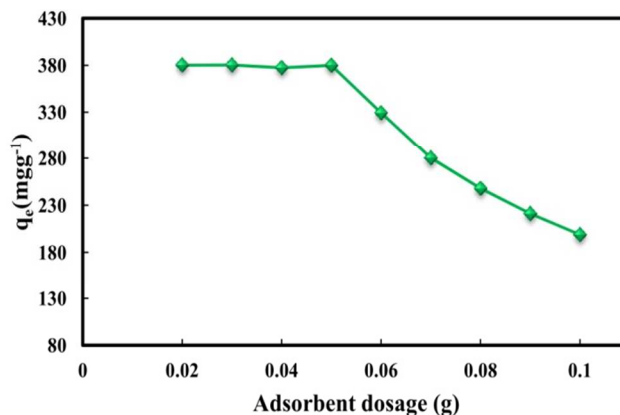
Fig.7 Effect of adsorbent dosage on the adsorption capacity of Pb^{2+} ions (Conditions: initial Pb^{2+} concentration: 50 mgL^{-1}, pH: 5.0, adsorbent dose: 1 gL^{-1}, contact time: 30 min, reaction temperature: 298.

As can be seen earlier (Figure 5), the functionalized nanoparticles show diminished affinity towards the target analyte at low pH. Hence, it is an indication that the adsorbent could be generated simply in an acidic environment. Therefore, several acids and their binary mixtures with different concentrations were evaluated to find the suitable eluent for simultaneous regeneration of the nanoadsorbent and recovery of the analyte. However, highly concentrated acids and their prolong contact with the AAA-NH$_2$-Si@MNPs can engulf the active species present on its surface and reduces its life span. Considering this verity, ultrasonic assisted mild acidic treatments were used to reduce the

extent of structural damage and to increase the lifetime of nanoadsorbent for multiple usage.

A contact time of 5 min was used as preset standard. It can be seen (Table ESI-S1) that Pb^{2+} desorption is highly favoured with HNO$_3$ in comparison to other desorptive reagents. Further, the metal recovery seems to get compromised, when nitric acid concentration and volume are less than 0.1 M and 4 mL respectively. The effective desorption of Pb^{2+} ions by HNO$_3$ has also been reported in the earlier studies,[20,33,34] which sustain our findings. To ensure the acidic resistance, the magnetic nanoadsorbent was suspended in 4 mL portions of 0.1 M nitric acid. Concentration of Fe, which was measured after 72 hours of contact time, showed negligible etching (<0.1ppm). This shows that Fe is strongly retained within the silica core, and the functionalized nanoparticles are highly stable towards encountered conditions. Thus, employed elution parameters are found to be optimum to concentrate and recover Pb^{2+} ions without impairing the stability of AAA-NH$_2$-Si@MNPs.

Effect of interfering ions

The prime source of competitive adsorption is the presence of different metal ions and electrolytes, which cause persistence hindrance to the binding affinity of analyte for the active sites and strongly inhibit the performance of functionalized nanoparticles. Besides this, the non-selective nature of adsorbents limits the reusability of heavy metal ions.[7] Recently, different materials have been reported for the efficient adsorption of Pb^{2+} ions, but they apparently lose their utility in real environmental application, as no attention has been paid to determine their selectivity behaviour in presence of other metals.[1,8,33] Thus, in the present study, the relevance of nanoadsorbent for the selective separation of Pb^{2+} ions from complicated matrices was assessed by treating the binary sample solutions containing 0.5 mgL^{-1} of Pb^{2+} ions, and varying concentration of interfering ions with pre-optimized experimental procedure. The analytical data, presenting the maximum tolerable concentration of the investigated ions causing a relative error of not more than 5% in the recovery of the target analyte, is as follows: 3.0 gL^{-1} K$^+$ and Na$^+$, 2.0 gL^{-1} Ca^{2+} and Mg^{2+}, 0.02 gL^{-1} Cd^{2+}, 0.04 gL^{-1} Cu^{2+}, Ni^{2+} and Co^{2+}, 0.05 gL^{-1} Zn^{2+}, 0.8 gL^{-1} Cr^{3+} and Fe^{3+} 1.0 gL^{-1} Al^{3+}, 2.0 gL^{-1} Cl$^-$, 5.0 gL^{-1} NO$_3{}^{2-}$ and CH$_3$COO$^-$ and 6.0 gL^{-1} SO$_4{}^{2-}$. It is evident from the results that AAA-NH$_2$-Si@MNPs possess high tolerance capacity to the various interfering cations and anions, which are inevitably associated with Pb^{2+} at trace levels.

This specificity and high affinity towards the target analyte can be explained on the basis of anchored organic functionalities over the surface of functionalized nanoparticles. As pointed out earlier, amide carbonyl and imine functional groups posses strong chelating ability for the analyte. This in turn leads to the selective adsorption of Pb^{2+} ions due to the formation of stable metal complex. In fact, the tendency of preferential uptake of Pb^{2+} on different adsorbents containing imine and carbonyl functional groups has already been reported in other studies.[29-31]

Besides functional groups, the other physiochemical properties of the metal ion can strongly influence the extent to which it binds to the material. Taking into consideration the concept of hydration enthalpy, it is the energy released when H$_2$O molecules in the solution attach themselves to the available metal ions.

The heavy metal which possesses lowest hydration energy can be transformed into bare ions most easily due to the ease of separation from the associated water molecules. It has the following sequence for the studied heavy metal ions: Al^{3+} > Cr^{3+} > Fe^{3+} > Ni^{2+} > Cu^{2+} > Co^{2+} > Zn^{2+} > Cd^{2+} > Pb^{2+}. As can be seen, Pb^{2+} has a lowest hydration enthalpy in comparison to other ions, which facilitates its easy availability to the existing functional groups on the surface of AAA-NH$_2$-Si@MNPs.[35,36] Thus, it can be efficiently and quickly captured by the nanoadsorbent even in a competitive metal environment. Likewise, both high electronegativity and ionic radius of Pb^{2+} in contrast to other ions can aid constructively for its selective adsorption (Table ESI-S2).[37]

Apart from these factors, earlier, Inoue *et al*. pointed out that the type of supporting material may significantly affect the selectivity behaviour of adsorbent.[38] Further, it was emphasized that the matrix may cause the orientation of the active sites in a manner to capture a particular metal ion having entirely unique physiochemical properties.[39] Indeed, the obtained results clearly demonstrate that the material substrate is positioning the active sites specific enough to particularly occupy Pb^{2+} ions and resulting in the formation of strong and stable metal chelate. Besides all these, the significance of experimental conditions to determine the selectivity cannot be subsided.[40] Hence, it can be inferred that the specificity of an adsorbent towards a particular metal is collectively dependent on all of the above mentioned parameters. In addition, due to the high tolerance to various interfering ions, the method can be successfully implemented to remove Pb^{2+} ions in the environmental samples.
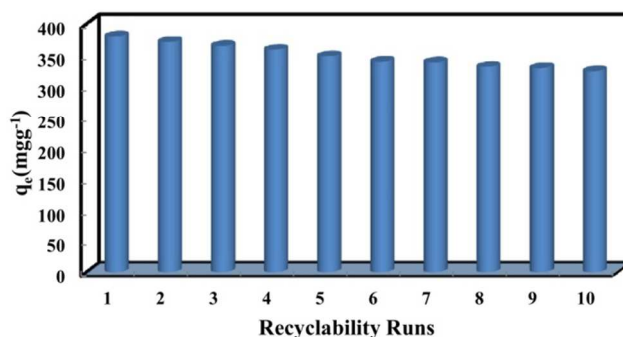
Fig. 8 The adsorption performance of AAA-NH$_2$-Si@MNPs by multiple regeneration cycles (Conditions: initial Pb^{2+} concentration: 50 mgL^{-1}, pH: 5.0, adsorbent dose: 1 gL^{-1}, contact time: 30 min, desorption time: 5min reaction temperature: 298 K).

Reusability

Besides an economic necessity, reusability of an adsorbent is an essential pathway to achieve the goal of sustainability, as it facilitates the continuous separation of heavy metals for their further recycling. But previously and in some of the recent work also, not much emphasis has been given to the reutilization of the adsorbents,[1,35,36] which limit their application for practical considerations. Therefore, in order to fulfil the purpose, ten successive adsorption-desorption runs using the same adsorbent were performed. Excellent recyclability and mechanical strength can be easily recognized by viewing the consistency in the performance of AAA-NH$_2$-Si@MNPs, in terms of adsorption capacity during each regeneration cycle (Figure 8). Besides, the

morphology and structure remain intact even after repetitive usage, and there is no sign of obvious agglomeration, which is demonstrated by the TEM and SEM image of the recovered functionalized nanoparticles (Figure ESI-S8). Likewise, the
5 saturation magnetization curve shows that the decrease in Ms

value is very less, in comparison to the fresh AAA-NH$_2$-Si@MNPs (Figure ESI-S9). This substantiates their good structural stability, which is not affected by the repeated stirring and acidic treatment throughout the cyclic process.
10

Table 4 Analysis of Pb^{2+} ions in different real samples (Conditions: pH: 5.0, adsorbent dose: 1 gL^{-1}, contact time: 30 min, desorption time: 5 min, reaction temperature: 298 K).

Sample	Added (µgL^{-1c} or µgg^{-1d})	Found (µgL^{-1} or µgg^{-1})	Recovery (%)
Yamuna river water	–	0.29 ± 0.01^e	–
	10.0	10.11 ± 0.16	98.3
Rain Water	–	5.72 ± 0.14	–
	10.0	15.76 ± 0.05	100.3
FA1^a	–	47.33 ± 0.58	–
	10.0	57.26 ± 0.80	99.9
FA2^a	–	46.76 ± 0.85	–
	10.0	56.02 ± 0.89	98.7
FA3^a	–	48.07 ± 1.18	–
	10.0	57.58 ± 1.12	99.2
FA4^a	–	47.94 ± 0.52	–
	10.0	57.10 ± 1.43	98.6
FA1^b	–	39.15 ± 0.50	–
	10.0	49.25 ± 0.88	100.2
FA2^b	–	41.84 ± 0.27	–
	10.0	51.26 ± 1.19	98.9
FA3^b	–	41.40 ± 0.52	–
	10.0	50.66 ± 0.99	98.6
FA4^b	–	40.86 ± 0.90	–
	10.0	50.34 ± 0.80	99.0

^{a} Mycorrhizal treated fly ash samples from Thermal Power Plant.

^{b} Mycorrhizal treated fly ash samples from Fertilizer Plant.

15 ^{c} For water samples.

^{d} For flyash samples.

^{e} Mean of five determinations $\pm ts/\sqrt{n}$ (t$_{4,0.05}$=2.78)

However, a perpetual but minor decline in the adsorption
20 capacity values of AAA-NH$_2$-Si@MNPs is observed during the ten cycles. It can be due to the partial loss of some of the active sites, to which Pb^{2+} ions are irreversibly bound leading to their unavailability for further adsorption. But even then, it adheres more than 85% of its original capacity in the final cycle. In fact,
25 the presence of the magnetic core makes the separation process very easy, and greatly reduces the loss of adsorbent with the repetitive usage. Thus, excellent reusability in conjunction with the high structural stability and efficiency of the nanoadsorbent for the removal of Pb^{2+} ions makes it a potential candidate to
30 combat ecological distress.

Application to real samples

The applicability of AAA-NH$_2$-Si@MNPs was tested in rain water, river water and mycorrhizal treated fly-ash samples. These environmental samples contain different miscellaneous ions,
35 which might compete for the interaction with nanoadsorbent. Consequently, validation was done by spiking a known amount of Pb^{2+} in the procured samples. The analytical results along with the recoveries for the spiked samples are represented through Table 4. Quantitative enrichment of trace level of Pb^{2+}, and
40 excellent agreement between the preconcentrated and spiked

values undoubtedly demonstrates the sensitivity, specificity and versatility of AAA-NH$_2$-Si@MNPs for extensive ecological applications.

Comparative analysis

45 To reassure the resourcefulness of the AAA-NH$_2$-Si@MNPs, its important analytical features have been compared with some recent literature citations and are listed in Table 5. As can be seen, the functionalized nanoparticles have very high loading capacity for preconcentration of Pb^{2+} ions. Although,
50 titanate/Fe$_3$O$_4$ nanocomposites[9] display a slightly enhanced quantitative binding capacity, but, the material we fabricate present a better capacity to be recycled, very less desorption time, fast kinetics and high specificity over other preconcentrating matrices. Also, the good reusability of EDTA modified
55 chitosan/SiO$_2$/Fe$_3$O$_4$ adsorbent[17] is superseded by the high adsorption capacity and low adsorption equilibrium time of the synthesized AAA-NH$_2$-Si@MNPs. In addition, when judged against non magnetic nanomaterials, the developed system possesses rapid and convenient operation and separation, and
60 economic dominance due to the existence of superparamagnetic inexpensive core material. In fact, the adsorbent is more compliant for practical purpose, due to the non-fragile nature of

silica protected MNPs, which enhances its durability and reusability in comparison to the adsorbents, where surface modifications are done on the bare iron oxide.[6,9,34]

Table 5 Various solid phase extraction systems for Pb^{2+} ions determination and their analytical characteristics.

Analytical technique	Adsorption capacity (mgg^{-1})	Reusability (cycle)	Equilibration/Elution time (min)	Ref.
Fe_3O_4-TETA-CMCS-FAAS	370.63	5	90/300	6
Ion-imprinted crown ether-AAS	27.95	5	60/120	7
Titanate/Fe_3O_4-ICPS	382.3	2	60/-	9
Fe_3O_4@SiO_2-NH_2-ICP-AAS	243.9	5	480/20	16
EDTA modified chitosan/SiO_2/ Fe_3O_4-MP-AES	123.5	12	720/600	17
Fe_3O_4@SiO_2@1,3-CalixCrown-ICP-AES	-	3	120/-	20
P(A-O)/AT nano-adsorbent-AAS	109.9	−	120/-	31
Fe_3O_4/cyclodextrin-ICP-MS	64.5	4	45/180	34
AAA-NH_2-Si@MNPs-FAAS	380.2	10	30/5	Present

Conclusions

The stepwise modification of iron oxide nanoparticles was performed to obtain a novel and effective magnetically driven multifunctional solid phase nanoadsorbent, which exhibited excellent performance for the lead removal. Superparmagnetic core provided ease of separation, while silica shell encapsulation endowed superior dispersibility and tenable strength to the nanoparticles, by preventing their aggregation and chemical decomposition. Exclusive selectivity towards the target analyte is due to the collective contribution of various factors, including anchored functional groups, material substrate, experimental conditions and physiochemical properties of the analyte. The assistance of sonication with mild acidic treatment in the elution process offers rapid recovery of Pb^{2+} ions without damaging the structure of functionalized nanoparticles. Cost effectiveness of embedded MNPs, good material stability, high adsorption capacity, ease of fabrication, and superior reusability over multiple adsorption/desorption cycles are some other valuable properties of AAA-NH_2-Si@MNPs. Thus, by the constructive integration of efficiency, selectivity and reusability, this finding paves a sustainable pathway for the systematic recovery and recycling of Pb^{2+} ions. Besides, the novel and unique applicability in mycorrhizal treated fly-ash samples can be envisioned as a powerful source to lower the leachable metal content to such an extent that the ecological stress is balanced.

Acknowledgements

Notes and references

a Green Chemistry Network Centre, Department of Chemistry, University of Delhi, Delhi-110007, India. Tel/Fax: +91-011-27666250 E-mail: rksharmagreenchem@hotmail.com

b Biotechnology and Management of Bioresources Division, The Energy and Resource Institute, New Delhi-110003, India. E-mail: aloka@teri.res.in

† Electronic Supplementary Information (ESI) available: [details of any supplementary information available should be included here]. See DOI: 10.1039/b000000x/

‡ Footnotes should appear here. These might include comments relevant to but not central to the matter under discussion, limited experimental and spectral data, and crystallographic data.

1. Y. L. F. Musico, C. M. Santos, M. L. P. Dalida and D. F. Rodrigues, *J. Mater. Chem. A*, 2013, **1**, 3789-3796.
2. T. E. Norgate and W. J. Rankin, The role of metals in sustainable development. In: Proceedings of green processing 2002. Cairns; 2002 pp. 49-55.
3. J. R. Dodson, A. J. Hunt, H. L. Parker, Y. Yang and J. H. Clark, *Chem. Eng. Process.*, 2012, **51**, 69-78.
4. WHO (2010), Exposure to lead: A major public health concern, Geneva, World Health Organization, Department of Public Health and Environment. (http://www.who.int/ipcs/features/lead..pdf).
5. WHO (2004). Lead exposure. In: Comparative quantification of health risks. Geneva, World Health Organization, pp. 1495-1542. (http://www.who.int/publications/cra/chapters/volume2/1495-1542.pdf).
6. S. P. Kuang, Z. Z. Wang, J. Liu and Z. C. Wu, *J. Hazard. Mater.*, 2013, **260**, 210-219.
7. X. Luo, L. Liu, F. Deng and S. Luo, *J. Mater. Chem. A*, 2013, **1**, 8280-8286.
8. Z. Ma, D. Zhao, Y. Chang, S. Xing, Y. Wu and Y. Gao, *Dalton Trans.*, 2013, **42**, 14261-14267.
9. F. Liu, Y. Jin, H. Liao, L. Cai, M. Tong and Y. Hou, *J. Mater. Chem. A*, 2013, **1**, 805-813.
10. S. S. Bayazit and I. Inci, *J. Ind. Eng. Chem.*, 2013, **19**, 2064-2071.
11. R. Sitko, E. Turek, B. Zawisza, E. Malicka, E. Talik, J. Heimann, A. Gagor, B. Feista and R. Wrzalik, *Dalton Trans.*, 2013, **42**, 5682-5689.
12. B Wang, H. Wu, L. Yu, R. Xu, T-T. Lim and X. W. (David) Lou, *Adv. Mater.*, 2012, **24**, 1111-1116.
13. R. K. Sharma, Y. Monga, A. Puri and G. Gaba, *Green Chem.*, 2013, **15**, 2800-2809.
14. A. H. Lu, E. L. Salabas and F. Schuth, *Angew. Chem. Int. Ed.*, 2007, **46**, 1222-1244.
15. R. K. Sharma, A. Puri, Y. Monga and A. Adholeya, *Sep. Purif. Technol.*, 2014, **127**, 121-130.

16. J. Zhang, S. Zhai, S. Li, Z. Xiao, Y. Song, Q. An and G. Tian, *Chem. Eng. J.*, 2013, **215-216**, 461-471.

17. Y. Ren, H. A. Abbood, F. He, H. Peng and K. Huang, *Chem. Eng. J.*, 2013, **226**, 300-311.

18. Y. Cui, J-Q. Liu, Z-J. Hu, X-W. Xu and H-W. Gao, *Anal. Methods*, 2012, **4**, 3095-3097.

19. B. Guo, F. Deng, Y. Zhao, X. Luo, S. Luo and C. Au, *Appl. Surf. Sci.*, 2014, **292**, 438-446.

20. R. Yi, G. Ye, D. Pan, F. Wu, M. Wen and J. Chen, *J. Mater. Chem. A*, 2014, **2**, 6840-6846.

21. R. K. Sharma, A. Puri, A. Kumar and A. Adholeya, *J. Environ. Sci.*, 2013, **25**, 1252-1261.

22. D. Ma, T. Veres, L. Clime, F. Normandin, J. Guan, D. Kingston and B. Simard, *J. Phys. Chem. C*, 2007, **111**, 1999-2007.

23. R. Abu-Reziq, H. Alper, D. Wang and M. L. Post, *J. Am. Chem. Soc.*, 2006, **28**, 5279-5282.

24. M. Yamaura, R. L. Camilo, L. C. Sampaio, M. A. Macedo, M. Nakamura and H. E. Toma, *J. Magn. Magn. Mater.*, 2004, **279**, 210-217.

25. V. S. Zaitsev, D. S. Filimonov, I. A. Presnyakov, R. J. Gambino and B. Chu, *J. Colloid Interf. Sci.*, 1999, **212**, 49-57.

26. L. M. Rossi, F. P. Silva, L. L. R. Vono, P. K. Kiyohara, E. L. Duarte, R. Itri, R. Landers and G. Machado, *Green Chem.*, 2007, **9**, 379-385.

27. C. H. Weng, *J. Colloid Interface Sci.*, 2004, **272(2)**, 262-270.

28. S. Yang, J. Hu, C. Chen, D. Shao and X. Wang, *Environ. Sci. Technol.*, 2011, **45(8)**, 3621-3627.

29. P. Chand and Y. B. Pakade, *J. Chem.*, 2013, 164575.

30. M. Mohammadhosseini and M. S. Tehrani, *J. Chin. Chem. Soc.*, 2006, **53**, 1119-1128.

31. X. Jin, C. Yu, Y. Li, Y. Qi, L. Yang, G. Zhao and H. Hu, *J. Hazard. Mater.*, 2011, **186**, 1672-1680.

32. A. Kaur and U. Gupta, *J. Mater. Chem.*, 2009, **19**, 8279-8289.

33. Y. Wang, J. Xie, Y. Wu, H. Ge and X. Hu, *J. Mater. Chem. A*, 2013, **1**, 8782-8789.

34. A. Z. M. Badruddoza, Z. B. Z. Shawon, T. W. J. Daniel, K. Hidajat and M. S. Uddin, *Carbohyd. Polym.*, 2013, **91**, 322-332.

35. W. Liu, T. Wang, A. G. L. Borthwick, Y. Wang, X. Yin, X. Li and X. J. Ni, *Sci. Total Environ.*, 2013, **456-457**, 171-180.

36. P. Trivedi and L. Axe, *Environ. Sci. Technol.*, 2001, **35**, 1779-1784.

37. X. Ma, L. Li, L. Yang, C. Su, K. Wang, S. Yuan and J. Zhou, *J. Hazard. Mater.*, 2012, **209-210**, 467-477.

38. K. Inoue, K. Yoshizuka and K. Ohto, *Anal. Chim. Acta*, 1999, **388**, 209-218.

39. L. F. Koong, K. F. Lam, J. Barford and G. McKay, *J. Colloid Interface Sci.*, 2013, **395**, 230-240.

40. E. Repo, J. K. Warchoł, A. Bhatnagar, A. Mudhoo and M. Sillanpaa, *Water Res.*, 2013, **47**, 4812-4832.